International Journal of Industrial Electronics, Control and Optimization © 2022 IECO
Vol. 5, No. 2, pp. 189-204, April (2022)

Adaptive Delay Compensator Based H_2/H_∞ Wide-Area Controller to Improve Damping of Inter-Area Oscillations

Esmaeel Rokrok [1,†], Saman Dehghaninejad [2], Amir Hossein Poursaeed [3]

[1,2,3] Department of Electrical Engineering, Lorestan University, Khorramabad, Iran

ABSTRACT

Recent technical advances in Wide-Area Measurement Systems (WAMS) have made it possible to use a combination of measured signals from remote locations to design centralized control. However, the transmission delay of remote signals and changes in the power system operating point are significant issues in the operation of the Wide-Area Damping Controller (WADC). Regarding issues and uncertainties in the power system, mixed H_2/H_∞ synthesis has been proposed for wide-area robust controller design. In this paper, an adaptive wide-area robust controller for Thyristor Controlled Series Capacitors (TCSC) is presented to improve the inter-area oscillation damping in multi-machine power systems in which the time-varying delays in feedback signal time are taken into account. So, an Adaptive Delay Compensator (ADC) is used to compensate for the delay of receiving remote signals. Despite the nonlinearity of the power system, the changes in the operating point, and the presence of time-varying delays, the proposed scheme shows robust performance in damping the low-frequency oscillations. The efficiency of the proposed control system in the presence of TCSC is shown through simulation results that show its superiority over the conventional control system. The simulation of the paper is carried out on the Four-Machine Two-Area test system and 10-machine, 39-bus New England power system.

Article Info

Research Article

Keywords:

Adaptive Robust Controller , Inter-Area Oscillation Damping, Time-Varying Delay ,Wide-Area Damping Controller

Article History:

Received 2021-11-28
Accepted 2022-05-19

I. INTRODUCTION

Once Damping inter-area modes of oscillation depend on different factors such as the system load level, the optimal transmission system design, the severity of the fault, and the type of system load [1]. Economically, power systems need to be operated near the system stability limit to reduce inter-area oscillations damping.

Also, the critical conditions are generated once the number of industrial loads and power electronics devices have increased, primarily constant power and constant current loads. Therefore, increasing the damping of inter-area oscillations is necessary to increase the transferable power using a suitable control strategy [2]. With the emergence and development of WAMS, many various controllers have been proposed to improve the performance of the power system [3]. Wide-Area Controller System (WACS) is used to improve the damping of inter-area oscillations which is called the Wide-Area Damping Controller (WADC). WADC for inter-area oscillation damping was first introduced in [4] under a hierarchical control structure, while Power System Stabilizers (PSSs) are used to stabilize local modes. WADC design method using wide-area signals can make it possible to select the optimal feedback signals with high observability from the inter-area modes of oscillation. As a result, WADC is more effective in damping inter-area oscillations than local controllers [5].

There is a time delay in transmitting feedback signals by a telecommunications channel from one place to another as an inherent feature of the WAMS. The delay depends on various factors such as the type of telecommunication channel, distance, and signal transmission protocol [6]. If the delay is

[†]**Corresponding Author**: rokrok.e@lu.ac.ir
Tel: +98-9166671706, Fax: +9866-33120088, Lorestan University
Department of Electrical Engineering, Lorestan University, Khorramabad,Iran

Copyright © 2022 Rokrok et al. Published by University of Sistan and Baluchestan. This work is licensed under a Creative Commons Attribution-Noncommercial 4.0 International license. (https://creativecommons.org/licenses/by-nc/4.0/). Non-commercial uses of the work are permitted, provided the original work is properly cited

not correctly considered in the controller design, it can affect WADC performance and system stability. The design method of conventional lead-lag compensators is presented to compensate for the phase change caused by the signal transmission delay in [7]. In [8] and [9], the methods based on Lyapunov stability theory are used to take the latency in the telecommunication channel into account. Also, the Smith Predictor is used to compensate for a certain amount of delay in [10]–[12], in which the linear model of the system is designed at an operating point. Therefore, the predictor may be ineffective in compensating for the delay once the system's operating point changes and leads to the production of an unstable signal.

Controllers designed using the aforementioned methods have constant parameters. So, these controllers will perform well only in small changes in latency. To ensure the optimal performance of the controller under abnormal operating conditions, it is necessary to compensate for the time-varying delay using adaptive approaches. Adaptive Delay Compensator (ADC) for wide-area robust damping controller design is presented in [13]–[16].

In [17], a robust multipurpose controller has been used to design the wide-area controller. For this purpose, the control scheme is based on the use of hierarchical control. Another limitation that poses a severe challenge to WADC implementation is the uncertainty in the system dynamic model. In [13]–[17], first, the structure which is used to implement WADC is introduced, then the multipurpose controller design method is investigated by mixed H_2/H_∞ synthesis and pole-placement using Linear Matrix Inequalities (LMI).

In this paper, an adaptive wide-area robust controller for TCSC is designed to improve the damping of inter-area oscillations in multi-machine power systems by considering the time-varying delay in the transmission of feedback signals. The structure of the topics of the article is as follows. Section II describes the modeling of different power system components, such as generator, excitation system, PSS, load, and TCSC. Section III introduces the design method of the robust inter-area controller. In section IV, the implementation of the proposed method for adaptive delay compensation is introduced. In section V, the results of the ADC-based wide-area controller for TCSC applied to the Four-Machine Two-Area test system and 39-bus New England power system are discussed. Finally, the conclusion is given in section VI.

II. MODELLING OF POWER SYSTEM COMPONENTS

performance as well as system stability. Power system dynamics and electrical relationships, which are described by differential equations, are nonlinear by nature. These equations represent the dynamical model of elements such as generators, excitation systems, governors, PSS, wind turbines, FACTS devices, etc. Generally, the power system can be expressed by a set of first-order differential and algebraic equations. With differential equations of power system components as well as the algebraic equations of the transmission network, the mathematical model of the whole system can be expressed by Eq. (1) [18], [19]:

$$\begin{cases} \dot{x_s} = f(x_s.d.u) \\ 0 \;\; = g(x_s.d.u) \\ y_s = h(x_s.d.u) \end{cases} \quad (1)$$

Where the vector function f defines the differential equations while g and h are the algebraic vector functions of the power system static equations. Also, x_s is the vector state variables of the system which is defined by Eq. (2).

$$\begin{aligned} x_s = [&\lambda_{1d1} \;\; \lambda_{1d2} \;\cdots\; \lambda_{1di} \,.\lambda_{2q1} \;\; \lambda_{2q2} \;\cdots \lambda_{2qi} \,. \\ &E'_{d1} \;\; E'_{d2} \cdots E'_{di}.E'_{q1} \;\; E'_{q2} \;\cdots E'_{qi}.\delta_1 \;\;\; \delta_2 \;\; . \\ &\omega_1 \;\; \omega_2 \;\; \cdots \;\; \omega_i. \;\; X_{1E1} \;\; X_{1E2} \;\; \cdots \;\; X_{1Ei}.X_{2E1} \;\; X_{2E2} \\ &X_{3E1} \;\; X_{3E2} \;\; \cdots \;\; X_{3Ei}.X_{tcsc}]^T \end{aligned} \quad (2)$$

Also, d is the vector of power system variables, as shown in Eq. (3).

$$\begin{aligned} &d \\ &= [\theta_1 \;\;\;\; \theta_2 \;\; \cdots \;\; \theta_{n_{bus}} \,.V_1 \;\;\;\; V_2 \;\;\; \cdots \;\;\; V_{n_{bus}} \,]^T \end{aligned} \quad (3)$$

Generally, the system inputs include governor reference, excitation system voltage, generator rotor speeds, and TCSC reference compensation percentage. In this paper, the reference voltage and rotor speed of the generators are considered the system's inputs, which are defined in Eq. (4).

$$u = [V_{WADCi} \;\;\; . \;\;\; X_{WADCi} \;]^T \;\;\; : i \in \{cg\} \quad (4)$$

cg refers to a set of controlled generators that damping of inter-area oscillations by applying control signals to their excitation system. Also, the static load model can be considered as Eqs. (5-6) [19]:

$$P_L(V) = \; P_0(A_1 + A_2\frac{V}{V_0} + A_3(\frac{V}{V_0})^2) \quad (5)$$

$$\mathrm{Q_L(V)} = \; \mathrm{Q_0(B_1 + B_2\frac{V}{V_0} + B_3(\frac{V}{V_0})^2)} \quad (6)$$

Where P_0 and Q_0 are the active and reactive load power at rated voltage V_0, respectively. Also, P_L and Q_L represent the active and reactive load power at V voltages, respectively. Also, the weighting factors $\mathrm{A_3}, \mathrm{A_2}, \mathrm{A_1(B_3}, \mathrm{B_2}, \mathrm{B_1)}$ represent the share percentage of active (reactive) load of constant impedance, constant current, and constant power, respectively. It should be noted that constant impedance and constant power load models are used in the Four-Machine Two-Area and 39-bus New England test systems, respectively. The relationship between these weighting factors must be established, as shown in Eq. (7).

$$\mathrm{A_1 + A_2 + A_3} = B_1 + B_2 + B_3 = 1 \quad (7)$$

The sub-transient model is also used to model the synchronous generators which are shown in Eqs. (8)-(13) [1].

$$T'_{d0i}\dot{E}'_{qi} = -E'_{qi} - (x_{di} - x'_{di})\left[i_{di} - \frac{x'_{di} - x''_{di}}{(x'_{di} - x_{li})^2}(\lambda_{1di} + (x'_{di} - x_{li})i_{di}) - E'_{qi}\right] + E_{fdi} \quad (8)$$

$$T''_{d0i}\dot{\lambda}_{1di} = -\lambda_{1di} + E'_{qi} - (x'_{di} - x_{li})i_{di} \quad (9)$$

$$T'_{q0i}\dot{E}'_{di} = -E'_{di} + (x_{qi} - x'_{qi})\left[i_{qi} - \frac{x'_{qi} - x''_{qi}}{(x'_{qi} - x_{li})^2}(\lambda_{2qi} + (x'_{qi} - x_{li})i_{qi}) + E'_{di}\right] \quad (10)$$

$$T''_{q0i}\dot{\lambda}_{2qi} = -\lambda_{2qi} - E'_{di} - (x'_{qi} - x_{li})i_{qi} \quad (11)$$

$$\dot{\delta}_i = \omega_i - \omega_s \quad (12)$$

$$2H_i\dot{\omega}_i = P_{mi} - (i_{qi}\lambda_{di} - i_{di}\lambda_{qi}) - K_{Di}(\omega_i - 1) \quad (13)$$

The IEEE type AC4A excitation system model is used in this paper. The block diagram of the excitation system is shown in Fig. 1 [18]. Differential equations that show the dynamic behavior of this type of excitation system defined as Eqs. (14)-(17).

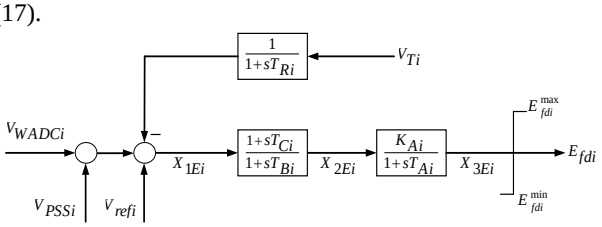


Fig. 1. IEEE type AC4A excitation system model

$$\dot{E}_{fdi} = \frac{K_{Ai}X_{2Ei}}{T_{Ai}} - \frac{1}{T_{Ai}}E_{fdi} \quad (14)$$

$$\dot{X}_{1Ei} = -\frac{1}{T_{Ri}}X_{1Ei} + \frac{1}{T_{Ri}}V_{Ti} \quad (15)$$

$$\dot{X}_{2Ei} = \frac{1}{T_{Bi}}\left(\frac{T_{Ci}}{T_{Ri}} - 1\right)X_{1Ei} - \frac{1}{T_{Bi}}X_{2Ei} - \frac{T_{Ci}}{T_{Bi}T_{Ri}}V_{Ti} + \frac{1}{T_{Bi}}(V_{WADCi} + V_{PSSi} + V_{refi}) \quad (16)$$

$$E_{fdi} = \begin{cases} E_{fdi}^{min} \\ X_{3Ei} \quad ; E_{fdi}^{min} \le X_{3Ei} \le E \\ E_{fdi}^{max} \end{cases} \quad (17)$$

The third-order model was used to design the PSS to stabilize the local modes of oscillations, as shown in Fig. 2. The rotor speed of the generator is used as an input signal to the PSS. So, Eqs. (18)-(20) represent the dynamic behavior of the PSS model.

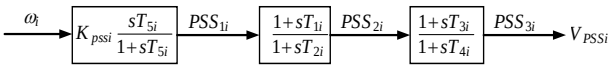


Fig. 2. Type PSS1A power system stabilizer model

$$P\dot{S}S_{1i} = -\frac{1}{T_{5i}}PSS_{1i} + K_{pssi}\frac{1}{120\pi}\dot{\omega}_i \quad (18)$$

$$P\dot{S}S_{2i} = -\frac{1}{T_{2i}}PSS_{2i} + \frac{1}{T_{2i}}PSS_{1i} + \frac{T_{1i}}{T_{2i}}P\dot{S}S_{1i} \quad (19)$$

$$P\dot{S}S_{3i} = -\frac{1}{T_{4i}}PSS_{3i} + \frac{1}{T_{4i}}PSS_{2i} + \frac{T_{3i}}{T_{4i}}P\dot{S}S_{2i} \quad (20)$$

Also, the dynamical model of TCSC considering the delay in thyristor firing angles is depicted by a lag compensator block in Fig. 3 [20]. Therefore, the output reactance changes can be expressed by Eqs. (21)-(24).

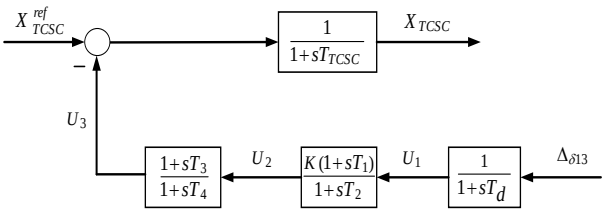


Fig. 3. TCSC block diagram

$$\dot{U}_0 = -\frac{1}{T_d}U_0 + \frac{1}{T_d}\Delta_{\delta 13} \quad (21)$$

$$\dot{U}_1 = -\frac{1}{T_2}U_1 + \frac{1}{T_2}KU_0 + \frac{T_1}{T_2}K\dot{U}_0 \quad (22)$$

$$\dot{U}_3 = -\frac{1}{T_4}U_3 + \frac{1}{T_4}U_1 + \frac{T_3}{T_4}\dot{U}_1 \quad (23)$$

$$\dot{X}_{tcsc} = -\frac{1}{T_{tcsc}}X_{tcsc} + \frac{1}{T_{tcsc}}X_{TCSC}^{ref} - \frac{1}{T_{tcsc}}U_3 \quad (24)$$

Where U_3 is a complementary control signal generated through a third-order dynamical model with generator rotor angle changes as its input. Also, the connection between the dynamic equations of the generators is established through the network admittance model. In the two-axis model of the synchronous generator, the dynamics of each machine are presented in a d-q reference frame that rotates at the speed of the machine rotor. To solve these equations, it is necessary to define a single reference frame for the whole system, called the system reference frame, and express all voltages and currents in that reference frame. The system reference frame rotates at synchronous speed. The voltage and current quantities of each machine can be expressed in the d-q reference frame of the machine or the system reference frame (R-I axes), as shown in Fig. 4. According to Fig.4, Eqs. (25) and (26) will be

established between the d-q and R-I quantities.

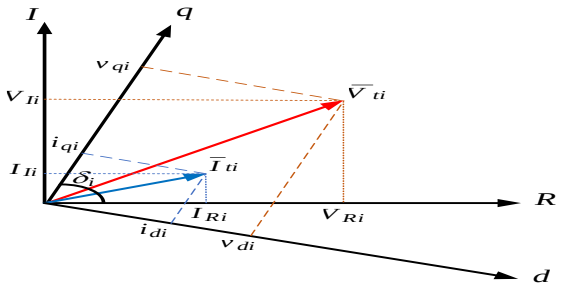


Fig. 4. The system reference frame and i^{th} generator reference frame

$$\bar{V}_{ti} = V_{Ri} + jV_{Ii} = (v_{di} + jv_{qi})e^{j(\delta_i - \frac{\pi}{2})} \quad (25)$$

$$\bar{I}_{ti} = I_{Ri} + jI_{Ii} = (i_{di} + ji_{qi})e^{j(\delta_i - \frac{\pi}{2})} \quad (26)$$

III. Wide-Area Damping Controller Design

This paper uses a robust multipurpose control based on [21] to design the wide-area controller. For this purpose, a two-level hierarchical control scheme is used with local controllers at the first level while the wide-area controller is implemented at the second stage. The hierarchical control scheme has minimum damping due to the performance of local controllers in the case of loss of telecommunications [3], [22]–[24].

The main goal of the multipurpose controller design is to use the combination of time and frequency domain performance of mixed H_2/H_∞ synthesis and defining the constraints of closed-loop poles placement in the desired location. In the design of the single-purpose H_∞ controller, robust stability, and elimination of output disturbance are achieved by H_∞ synthesis. In the multipurpose controller design of mixed H_2/H_∞ synthesis, the H_∞ synthesis is only used to obtain robust stability against model uncertainty, while the elimination of output disturbance with considered limitations is carried out by H_2 synthesis. So, the multipurpose controller has a better transient response than the single-purpose scheme. The block diagram of the closed-loop system with WADC utilizing the multipurpose design is shown in Fig. 5, where u_{wadc} and y_{wadc} represent the wide-area controller's input vector and output vector, respectively [25].

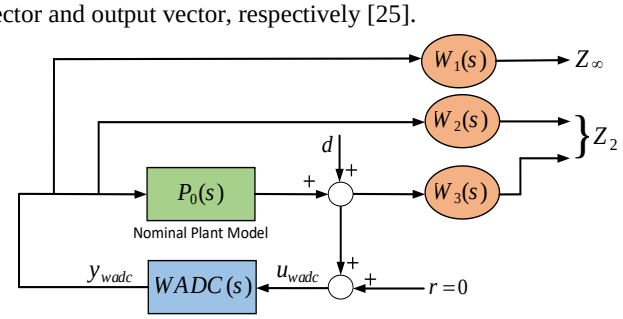


Fig. 5. Multipurpose controller design using weighting functions

In Fig. 5, the output channel z_∞ corresponds to optimizing the H_∞ performance while the output channel z_2 aims to improve the H_2 performance. Also, $W_3(s)$, $W_2(s)$ and $W_1(s)$ are the weighting functions in the frequency domain. The $W_3(s)$ function, which is in the z_2 channel, is a low-pass filter used to eliminate the disturbance effect on the output. Also, the weighting function $W_2(s)$ is a high-pass filter which usually is considered as a small constant number to minimize the disturbance effect on the controller output. Finally, the weighting function $W_1(s)$, which is in the output channel of Z_∞, is a high-pass filter used to robust stability against the model uncertainty. Furthermore, $P_0(s)$ is the nominal plant of the system which is obtained by the reduced model of the power system. The delay has been considered in this system linear model [15]. So, the system shown in Fig. 5 can be shown as a Linear Fractional Transformation (LFT) model in Fig. 6, where $\tilde{P}_0(s)$ represents the modified plant model with weighting functions.

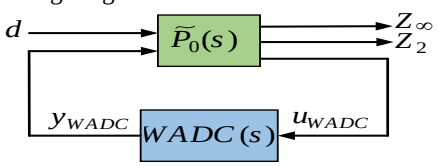


Fig. 6. LFT block diagram for the multipurpose design approach

$$\begin{cases} \dot{x}_P = A_P x_P + B_{Pd} d + B_P y_{wadc} \\ z_\infty = C_x x_P + D_{dx} d + D_x y_{wadc} \\ z_2 = C_2 x_P + D_{d2} d + D_2 y_{wadc} \\ y_s = u_{wadc} = C_P x_P + D_{pd} d \end{cases} \quad (27)$$

$$\begin{cases} \dot{x}_k = A_k x_k + B_k u_{wadc} \\ y_{wadc} = C_k x_k + D_k u_{wadc} \end{cases} \quad (28)$$

So, state-space equations of the closed-loop system can be expressed in Eq. (29).

$$\begin{cases} \dot{x}_{cl} = A_{cl} x_{cl} + B_{cl} d \\ z_\infty = C_{cl1} x_{cl} + D_{cl1} d \\ z_2 = C_{cl2} x_{cl} + D_{cl2} d \end{cases} \quad (29)$$

Where x_{cl}, C_{cl1}, and C_{cl2} are defined as Eqs. (30)-(32), respectively.

$$x_{cl} = \begin{pmatrix} x_p \\ x_k \end{pmatrix} . A_{cl} = \begin{pmatrix} A_P + B_P D_K C_P & B_P C_K \\ B_K C_P & A_K \end{pmatrix} . \begin{pmatrix} B_{pd} + B_p D_k D_{pd} \\ B_k D_{pd} \end{pmatrix} \quad (30)$$

$$C_{cl1} = \begin{pmatrix} C_\infty + D_\infty D_k C_p & D_\infty C_k \end{pmatrix}. \quad D_{cl1} = D_{d\infty} + D_\infty D_k D_{pd} \quad (31)$$

$$C_{cl2} = \begin{pmatrix} C_2 + D_2 D_k C_p & D_2 C_k \end{pmatrix}. \quad D_{cl2} = D_{d2} + D_2 D_k D_{pd} \quad (32)$$

According to Fig. 5, the main objectives of WADC design are as follows. 1) Improve H_∞ synthesis performance to controller robustness against system uncertainties, 2) Improve H_2 synthesis performance to improve controller performance

once the system is subjected to large disturbances, 3) Placement of the closed-loop poles in a specific location on the left-half plane to achieve a desired transient response. In mathematical terms, multipurpose controller design can be expressed as an optimization problem that minimizes mixed H_2/H_∞ synthesis, which is displayed as Eq. (33).

$$\begin{aligned} &Minimize\ \ a_\infty \left\|T_{dz_\infty}(s)\right\|_\infty^2 + a_2 \left\|T_{dz_2}(s)\right\|_2^2 \\ &subject\ \ to: \\ &poles\ \ \in region \end{aligned} \tag{33}$$

Where $T_{dz_\infty}(s)$ and $T_{dz_2}(s)$ are the closed-loop transfer functions of the disturbance d to the outputs z_∞ and z_2, respectively. $\left\|T_{dz_\infty}(s)\right\|_\infty$ and $\left\|T_{dz_2}(s)\right\|_2$ represent the H_∞ and H_2 norms of the $T_{dz_\infty}(s)$ and $T_{dz_2}(s)$ transfer functions, respectively. Also, a_∞ and a_2 weighting factors. To achieve the desired transient response, it is necessary to place the closed-loop poles in the left-half plane. This specific location for the placement of closed-loop poles is considered according to Fig. 7. Therefore, the maximum settling time and the minimum inter-area oscillation damping ratio will be limited to $4/a$ and $\cos(\beta)$, respectively.

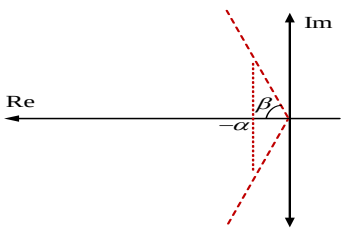


Fig. 7. The region of interest for the pole-placement of the closed-loop system

IV. Adaptive Delay Compensator for Wide-Area Robust Controller Design

An ADC for the robust controller system to dampen the inter-area oscillations has been presented. The implementation of the proposed method contains two main steps: 1) To design an ADC, First, ADC is defined as the weighted sum of several phase compensators with the consideration of the delay variation range. Then, the weighting factors are adjusted in real-time according to the measured delay value to compensate for the time-varying delay. 2) To design the robust controller, the delay compensator is considered as a part of the controlled system, and the WADC controller is designed using the method as mentioned above described in Section III to improve the damping of inter-area oscillations.

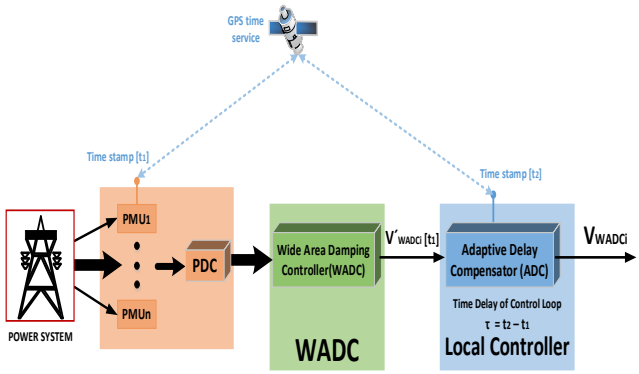


Fig. 8. Control structure based on generator excitation system with ADC

The most crucial point to remember about continuous-time delay compensation is the robustness of WADC against delay changes. However, the ADC can easily extract the delay model and use it to design WADC and its robustness against delay changes. The delay caused by signal transmission becomes even more critical once the used control scheme is the wide-area controller [26]. The structure of the wide-area control system with the ADC is shown in Fig. 8. PMU measurements are collected at t_1 and synchronized in Phasor Data Concentrator (PDC) [27]. When one or more telecommunications links become overloaded, the PDC waits until it receives all the signals with timestamp t_1 and sends feedback signals to the WADC after the measured signals are synchronized. After receiving the feedback signals, WADC calculates the control signal V'_{WADC_i} with the timestamp t_1 and sends it to the ADC located at the control center. When ADC receives control signal V'_{WADC_i} (corresponds to timestamp t_1), the control loop delay is calculated as $\tau = t_2 - t_1$, where t_2 represents the new timestamp currently that the control signal reaches the delay compensator. Also, it is determined in real-time by the Global Positioning System (GPS). So, the ADC generates the appropriate phase value to compensate for the measured delay. Then, the compensated signal V_{WADCi} is applied to the Automatic Voltage Regulator (AVR) input mounted on the synchronous generator excitation system or FACTS compensator to achieve desirable dynamical performance. In this paper, the ADC performance is evaluated in a wide-area control system on the TCSC. Also, it is assumed that the WADC is located near of the TCSC installed location. So, the proposed control scheme is shown in Fig. 9. In the presented scheme, ADC receives the feedback signal M (corresponds to timestamp t_1) from the data center. ADC performs the phase compensation concerning measured delay and applies the compensated signal to the WADC input. So, WADC calculates the control signal X_{WADC} and apply it to TCSC to improve the damping of inter-area oscillations.

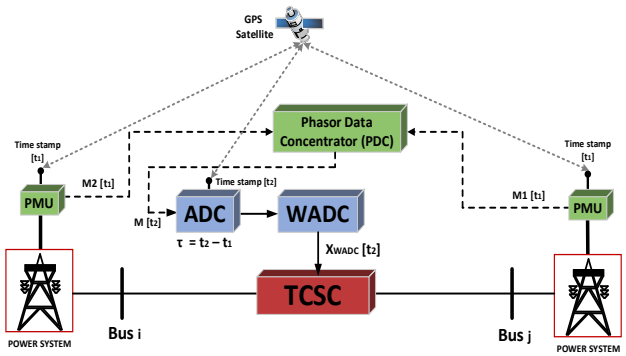


Fig. 9. The proposed control scheme based on TCSC usage with ADC

A. *The delay of the WAMS communication network*

The delays in the WAMS communication network are caused by the measurements' processing time, synchronization, sending of measurement signals, calculation of control signals, and sending them. Therefore, the total delay is equal to the time it takes to send a measured signal by the PMU to the control center. Conventional telecommunication lines in the WAMS are generally divided into two categories; wired links and wireless links. Satellite and digital microwave links are the most used wireless links, while fiber-optic lines, Power Line Carriers (PLCs), and telephone lines are among the most common wired links. The delay for these conventional telecommunication lines is shown in Table I[28], [29].

TABLE I
DELAY FOR VARIOUS TELECOMMUNICATION LINES IN THE WAMS SYSTEM [30]

Telecommunication line type	Delay (milliseconds)
Fiber optic lines	100-150
Digital microwaves	100-150
Power line carrier	150-350
Telephone lines	200-300
Satellite	500-700

B. *Delay modeling*

The most widely used approach of delay modeling is to approximate it with a transfer function in a specific frequency range. The delay transfer function is generally defined as Eq. (34). A common approach used for delay modeling is the Pade Approximation of order n of the delay, which is presented as Eq. (35) [15].

$$G_d(s) = e^{-\tau s} \tag{34}$$

$$G_d^n(s) = \frac{\sum_{k=0}^{n} \frac{(-1)^k (2n-k)!nl}{2n!k!(n-k)!} \tau^k s^k}{\sum_{k=0}^{n} \frac{(2n-k)!nl}{2n!k!(n-k)!} \tau^k s^k} \tag{35}$$

The approximated delay model is obtained by Eq. (36).

$$G_D(s) = \frac{(1-\frac{s\tau}{2n})^n}{(1+\frac{s\tau}{2n})^n} \tag{36}$$

C. *Adaptive Delay Compensation Design*

The proposed ADC is a weighted sum of several compensators in which the weighting factor corresponds to each compensator is updated in continuous time according to the measured delay. To describe the ADC process, $\bar{G}_D(s)$ considered as a minimum phase transfer function, as shown in Eq. (37).

$$\bar{G}_D(s) = \frac{1}{(1+\frac{s\tau}{2n})^{2n}} \tag{37}$$

The phase of the $\bar{G}_D(s)$ the transfer function is the same as the approximate delay model phase expressed by the Eq. (36). Therefore, the transfer function of each compensator using $\bar{G}_D(s)$ is defined by Eq. (38).

$$DC_i(s) = K(T_i)\frac{\left(1+\frac{sT_i}{2n}\right)^{2n}}{(1+sT_c)^{2n}} \qquad i = 1,2,\cdots,m \tag{38}$$

Where $DC_i(s)$ represents the i^{th} compensator transfer function, m shows the number of compensators, T_i and T_c are the phase lead (numerator) and phase lag (denominator) time constants of the are i^{th} compensator, respectively. Also, K is the Gain Correction Factor (GCF), a function of the delay. So, the state-space equations of the compensators can be expressed using controllable canonical realization. The i^{th} compensator state-space equations will be defined as Eqs. (39) and (40).

$$\dot{x}_{ADC}(t) = A_{ADC}x_{ADC}(t) + B_{ADC}u_{ADC}(t) \tag{39}$$

$$y_{DC_i}(t) = C_{DC_i}x_{ADC}(t) + D_{DC_i}u_{ADC}(t) \tag{40}$$

Where A_{ADC} and B_{ADC} are state matrices and delay compensator inputs, respectively. Also, C_{DC_i} and D_{DC_i} are the output and direct supply matrices of the i^{th} compensator, respectively. x_{ADC} is the state variable vector of delay compensator, u_{ADC} represents the remote signal applied to the compensator input, and finally, y_{DC_i} represents the output of the i^{th} compensator. The proposed ADC is considered as a weighted sum of a small number of compensators where its transfer function is indicated in Eq. (41).

$$ADC(s) = \frac{N(s)}{D(s)} = \sum_{i=1}^{m} \beta_i(\tau) DC_i(s) \tag{41}$$

Where $N(s)$ and $D(s)$ are the polynomials of the numerator and denominator of ADC, respectively. Also, $\beta_i(\tau)$ is the weighting factor of the i^{th} compensator. If m is the number of compensators, then the weighting factors used in Eq. (41) can be obtained by Eq. (42).

$$\bar{\beta}(\tau) = \bar{T}^{-1}\bar{T}_\tau \tag{42}$$

Where $\bar{\beta}(\tau)$, $\bar{T}$, and $\bar{T}_\tau$ are expressed as Eqs. (43)-(45).

$$\bar{\beta}(\tau) = [\beta_1(\tau) \quad \beta_2(\tau) \quad \cdots \quad \beta_m(\tau)]^{\mathrm{T}} \tag{43}$$

$$\bar{T} = \begin{pmatrix} 1 & 1 & \cdots & 1 \\ T_1 & T_1 & \cdots & T_m \\ T_1^{\,2} & T_2^{\,2} & \cdots & T_m^{\,2} \\ \vdots & \vdots & \ddots & \vdots \\ T_1^{\,m-1} & T_2^{\,m-1} & \cdots & T_m^{\,m-1} \end{pmatrix} \tag{44}$$

$$\bar{T}_\tau = \begin{pmatrix} 1 \\ \tau \\ \tau^2 \\ \vdots \\ \tau^{m-1} \end{pmatrix} \tag{45}$$

The implementation of the proposed ADC is shown in Fig. 10, where matrices $\bar{C}_{ADC}$ and $\bar{D}_{ADC}$ are defined as Eqs. (46) and (47), respectively.

$$\bar{\mathrm{C}}_{\mathrm{ADC}} = [\mathrm{C_{DC1}}^{\mathrm{T}} \quad \mathrm{C_{DC2}}^{\mathrm{T}} \quad \cdots \quad \mathrm{C_{DCm}}^{\mathrm{T}}]^{\mathrm{T}} \tag{46}$$

$$\bar{\mathrm{D}}_{\mathrm{ADC}} = [\mathrm{D_{DC1}}^{\mathrm{T}} \quad \mathrm{D_{DC2}}^{\mathrm{T}} \quad \cdots \quad \mathrm{D_{DCm}}^{\mathrm{T}}]^{\mathrm{T}} \tag{47}$$

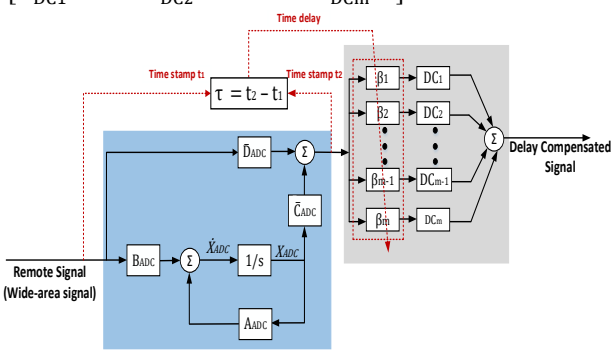


Fig. 10. The proposed ADC

The block diagram of the closed-loop system by considering WADC and ADC is depicted in Fig. 11. In this figure, $G_0(s)$ represents the linearized model of the power system, and the compensated delay model is represented by $CDM_t(s)$. To implement the ADC using Eq. (41), the compensated delay model will be represented as Eq. (48) [27].

$$\mathrm{CDM_\tau(s) = ADC(s)G_D(s)} = \frac{\sum_{i=1}^{m}\beta_i(\tau)\mathrm{K(T_i)}\left(1+\frac{\mathrm{sT_i}}{2n}\right)^{2n}}{(1+\mathrm{sT_c})^{2n}} \frac{(1-\frac{s\tau}{2n})^n}{(1+\frac{s\tau}{2n})^n} \tag{48}$$

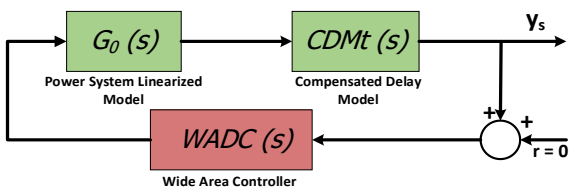


Fig. 11. Closed-loop system block diagram considering WADC and ADC

By considering the ADC, the common point of the system linearized and compensated delay models are considered the plant that the WADC is designed. The plant for the above-mentioned system displayed in Fig. 11 is defined as Eq. (49).

$$\mathrm{P(s) = G_0(s)CDM_\tau(s)} \tag{49}$$

V. Simulation Results

A. Case Study I: Four-Machine Two-Area Test System

To show the advantages of TCSC-based WADC performance, the proposed control scheme was applied to the Four-Machine Two-Area test system, which is shown in Fig. 12. It should be noted that PSSs are only installed on G1 and G3 generators, while PSSs for G2 and G4 generators have not been considered. The transfer function of the PSSs as mentioned earlier and the conventional wide-area controller are shown in Eqs. (50) and (51), respectively.

$$H_{PSS}(s) = 8\frac{7s}{1+8s}\left(\frac{1+008s}{1+003s}\right)^2 \tag{50}$$

$$H_{WADC}(s) = K_a\frac{7s}{1+8s}\left(\frac{1+0.08s}{1+0.03s}\right)^2 \tag{51}$$

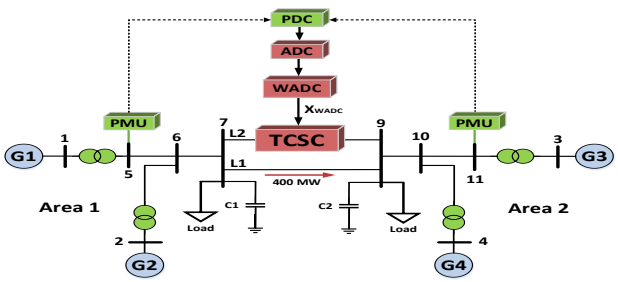


Fig. 12. Single line diagram of two area four machine system with TCSC

TABLE II
TIME-VARYING DELAY CONSIDERED

Time Interval (s)	Time Delay (ms)
$0 \le t < 7$	$470 \pm \theta_\tau$
$7 \le t < 10$	$150 \pm \theta_\tau$
$10 \le t \le 20$	$290 \pm \theta_\tau$

Where K_a is selected based on a trade-off between the delay margin and the damping performance. The time-domain simulations are carried out to show the performance of the proposed WADC in the presence and absence of TCSC once the system is subjected to a large disturbance. The simulation results for the three-phase fault that occurred on the L2 line for different delay values are shown in Fig. 13. The three-phase to fault occurs at 0.1 s while it is cleared after 0.1 s. Also, the assumed time-varying delay is considered in Table II, where θ_τ is a random value between zero and 30 ms. As shown in Fig. 13, the adaptive wide-area robust controller has a great performance in damping inter-area oscillations against the different values delay compared to the other methods. When the delay is 100 ms, the ADC is equal to the DC1 compensator, and the performance of the lead-lag controller with $K_a = 4$ is approximately similar to the performance of the proposed method. However, the performance of the conventional

controller completely deteriorates with an increase in delay value and time-varying delay. On the other hand, the controller with $K_a = 2$ gain can withstand a more extensive range of delay changes because its delay margin is 358 ms. As can be seen, this enhancement in the delay margin is obtained by weakening the controller damping performance where damping of the oscillations is last more than 20 s with different values of time delay. Although this gain provides an enhanced damping ratio for the lead-lag controller compared to the open-loop system, the desirable damping is not preserved in either low or high values of delay.

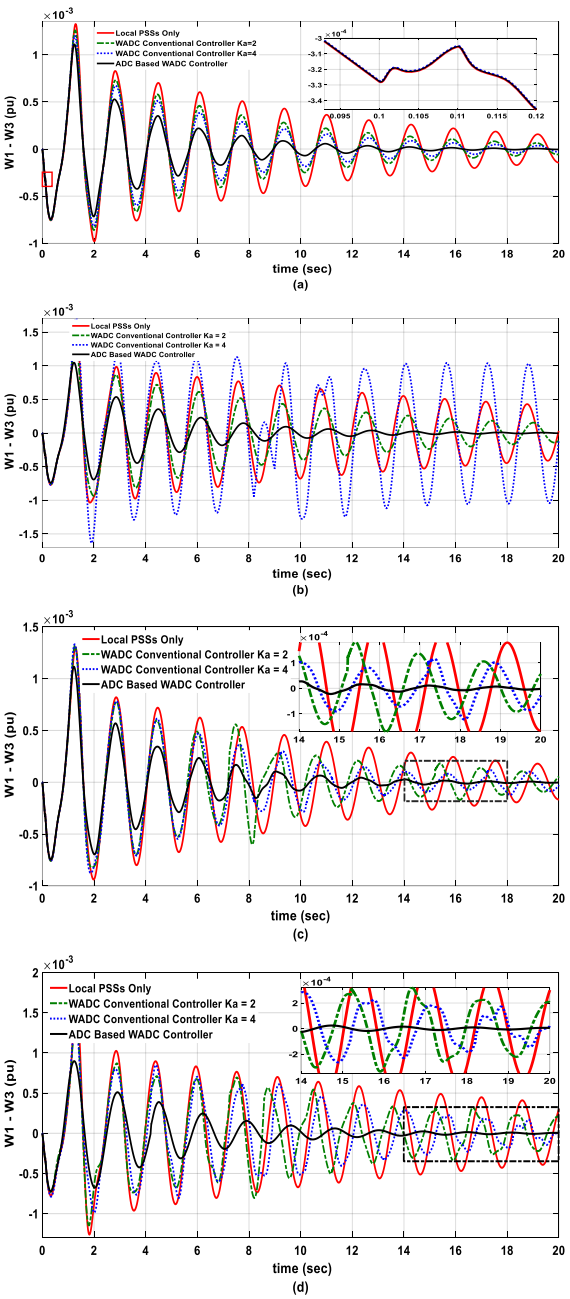


Fig. 13. The rotor speed changes of the G1 and G3 subjected to a 3-phase fault on the L2 line (a) delay =100 ms (b) delay =300 ms, (c) delay =500 ms, (d) time-varying delay.

Also, Fig. 14 shows the simulation results of the G1 and G3 generators' speed changes caused by different delays with ADC-based centralized controller and PSS. As can be seen, the ADC-based WADC has appropriate damping at different time delays than the fixed-delay compensators (DC1, DC3, and DC5) and PSS.

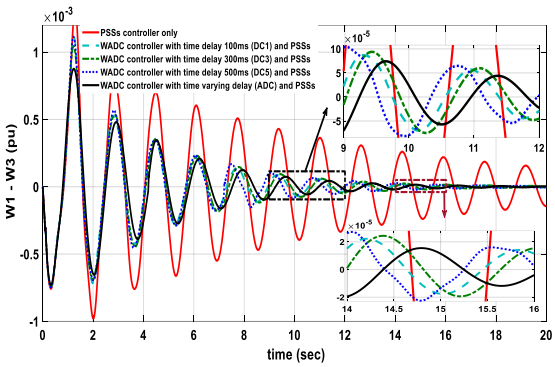


Fig. 14. Different delays with ADC-based centralized controller caused the rotor speed changes of the G1 and G3

Small signal analysis for the Two-Area test system in the presence and absence of TCSC shows that the system has three oscillatory modes. The participation of each generator in these oscillatory modes is shown in Tables III and IV. As can be seen, the damping ratio of all electromechanical modes as well as the frequency of local modes has changed. However, the inter-area mode frequency increased from 0.7344 Hz to 0.7515 Hz. This mode has a settling time of 30 s because of its damping ratio and low oscillation frequency. So, it is essential to improve the damping ratio of this oscillatory mode.

TABLE III
ELECTROMECHANICAL MODES OF TWO-AREA SYSTEM WITHOUT TCSC

Local and inter-area modes value	Mode shape	Damping ratio (%)	Frequency (Hz)	Mode
$-0.6467 \pm 4.6711i$	G1, G2 VS. G3, G4	13.71	0.7344	1
$-5.8336 \pm 12.298i$	G3 VS. G4	42.86	1.9573	2
$-4.7517 \pm 13.7841i$	G1 VS. G2	32.59	2.1938	3

TABLE IV
ELECTROMECHANICAL MODES OF TWO-AREA SYSTEM WITH TCSC

Local and inter-area modes value	Mode shape	Damping ratio (%)	Frequency (Hz)	Mode
$-0.7349 \pm 4.7116i$	G1, G2 VS.G3,G4	15.41	0.7515	1
$-5.8698 \pm 12.4025i$	G3 VS. G4	42.78	1.9739	2
$-4.7804 \pm 13.9393i$	G1 VS. G2	32.44	2.2185	3

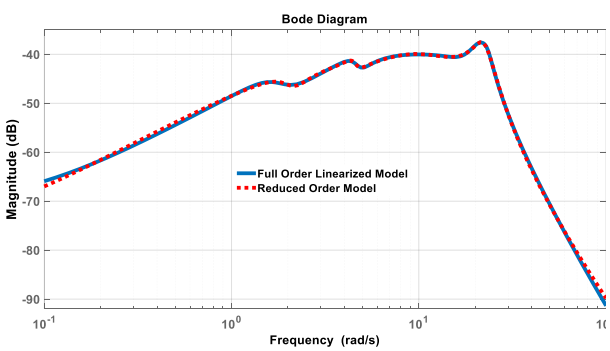
The considered feedback signals are the speed changes of the generators in the system. The inter-area mode damping is done by applying a control signal to the generator excitation system. The relative values of the inter-area mode for different feedback signals and control locations are shown in Table V. According to the results, the G1 generator is considered the control location, and the speed changes between the G1 and G3 generators, which have the highest visibility of the inter-area mode, are selected as the feedback signal. In this work, the WADC is located near the TCSC while ADC is installed to compensate for the delay in the feedback signal.

TABLE V

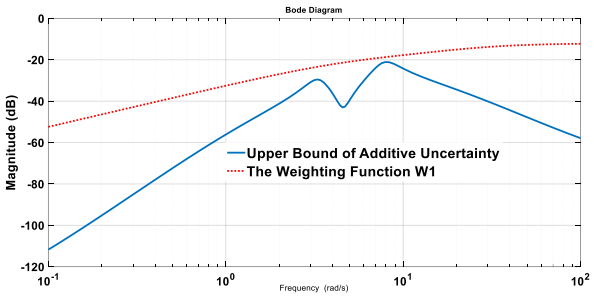
FEEDBACK SIGNALS AND CONTROL LOCATIONS

		Feedback Signal					
		$\omega_1 - \omega_2$	$\boldsymbol{\omega_1 - \omega_3}$	$\omega_1 - \omega_4$	$\omega_2 - \omega_3$	$\omega_2 - \omega_4$	$\boldsymbol{\omega_3 - \omega_4}$
Control Location	G1	0.0561	**1.0000**	0.9038	0.8175	0.8178	0.0409
	G2	0.0506	0.8148	0.7984	0.7138	0.7581	0.0385
	G3	0.0423	0.8506	0.6417	0.5163	0.5896	0.0289
	G4	0.0473	0.7124	0.7064	0.6791	0.6302	0.0353

The order of the linearized model obtained by MATLAB software is 55, which is reduced to 10 using the Schur model order reduction method [31]. The bode diagram for the original model and reduced model are shown in Fig. 15 (a). As can be seen, the reduced model in the frequency range of the electromechanical oscillations has the same dynamic behavior as the original model. The delay variation is considered between 100 ms and 500 ms. Also, the time constants of these compensators are considered as T_1 =0.1, T_2 =0.2, T_3 =0.3, T_4 = 0.4, T_5 = 0.5. The variations in the delay will cause uncertainty in the compensated delay model. The main part of this uncertainty is due to the variation in the gain value of this model, which if GCF is not used, the gain increases with increasing of the delay value and decreases with decreasing of the delay value. Therefore, using an appropriate gain factor can reduce the caused uncertainty by delay variations. The MSV diagram of the designed plant considering the uncertainty is shown in Fig.15 (b).



(a)



(b)

Fig. 15. (a) Bode plot of the linearized model and reduced model (b) MSV diagram for $W_1(s)$ weighting function and plant uncertainty

Also, the weighting functions $W_1(s)$,$W_2(s)$,$W_3(s)$ are considered as Eqs. (52) - (54) [32].

$$W_2(s) = 02 \tag{52}$$

$$W_3(s) = \frac{10}{s+20} \tag{53}$$

$$W_1(s) = 8s/(s+90) \tag{54}$$

The weighting factors of H_∞ and H_2 are assumed 0.5. The results of the controller design are presented in Table VI.

TABLE VI

THE DESIGNED CONTROLLER WITH TCSC BY CONSIDERING $a = 0.49$ AND $\beta = 87$ FOR THE LMI REGION

Designed controller with TCSC	
$\|\|T_{dz_\infty}\|\|_\infty$	$\|\|T_{dz_2}\|\|_2$
0.786	0.244

The time-varying delay, the weighting factors of compensators, and the ADC output signal applied to the AVR input of the G1 generator are shown in Fig. 16. This figure shows the ADC output variations between the outputs of other compensators when a large latency variation occurs.

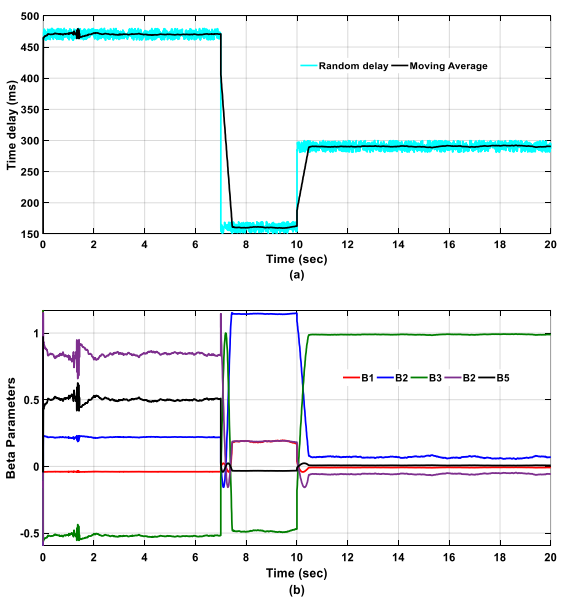


Fig.16 . Continued

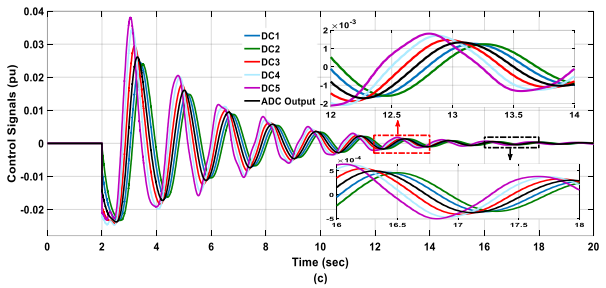


Fig. 16. Vertex compensator weights and control signals. (a) Time-varying delay, (b) Weight of vertex compensators, (c) the output of vertex compensators and ADC

Also, Fig. 17 shows the rotor speed changes of the G1 and G3 caused by different delays with ADC-based centralized controller and TCSC. As can be seen, the ADC-based WADC with TCSC has suitable damping at different time delays than the fixed-delay compensators (DC1, DC3, and DC5).

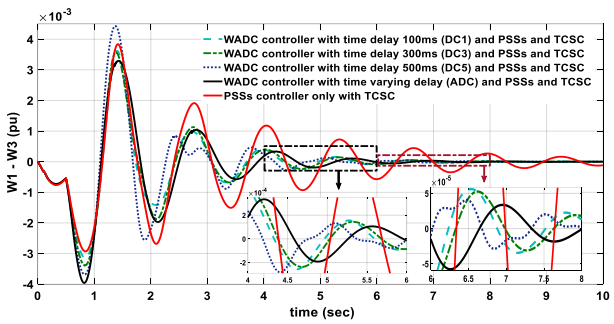
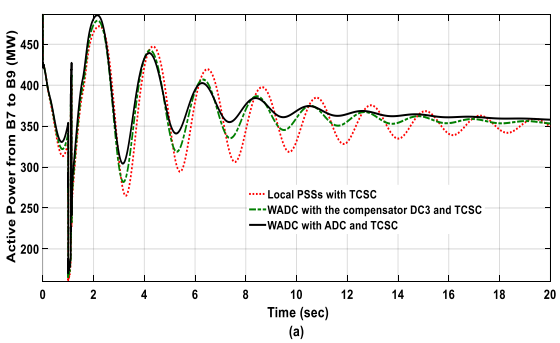
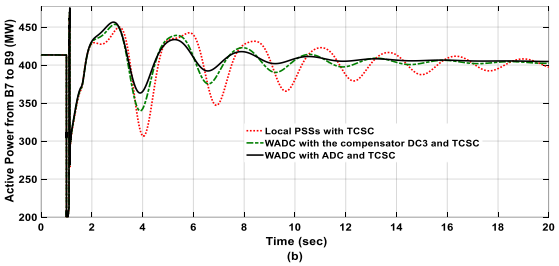


Fig. 17. The rotor speed changes of the G1 and G3 were caused by different delays with an ADC-based centralized controller and TCSC

Fig. 18 shows the active power from bus 7 to bus 9 with fault levels and different operating conditions. A three-phase to fault occurs at 1 s on the L2 line, and it is cleared after 0.1 s. Fig. 18 (a) shows the active power from bus 7 to bus 9 considering 80% of the load, Fig. 18 (b) shows 100% of the load, and Fig. 18 (c) shows 120% of the loads. As can be seen, WADC based ADC with TCSC compared to WADC with 300 ms fixed-delay compensator and PSSs have better performance.





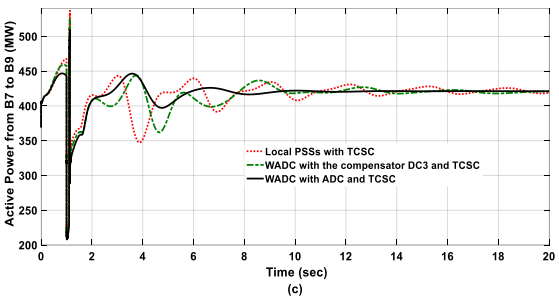


Fig. 18. The occurrence of 3-phase to fault on the L2 line at different operating points with the presence of TCSC (a) 80% load (b) 100% load (c) 120% load

B. Case Study II: 39-Bus 10-Machine Power System

The IEEE 39-bus 10-machine system with TCSC is chosen to evaluate the performance of the proposed method in a wide-area controller based on the use of FACTS devices. The single-line diagram of the network is shown in Fig. 19. This system consists of 10 synchronous generators, in which the G1 generator represents the dynamic model of the external grid. To impose the stress on the system, the load level and the generation have been increased. The local PSSs are installed only on generators G2, G3, G5, G8, and G9, while other generators are not equipped with PSS. The PSS transfer function installed on the aforementioned generators is displayed in Table VII [33], [34].

Small signal analysis of the linearized model of the system, according to Table (8), shows that the system has four oscillatory modes with a frequency of less than one Hz. Since, in each of these oscillatory modes, several generators oscillate against each other, they can be considered inter-area oscillation modes. Corresponding generators that produce these oscillatory modes include five groups of coherent generators. As shown in Table VIII, the groups mentioned above of coherent generators consist of G9, (G2 and G3), (G4, G5, G6, and G7), (G8 and G10), and G1.

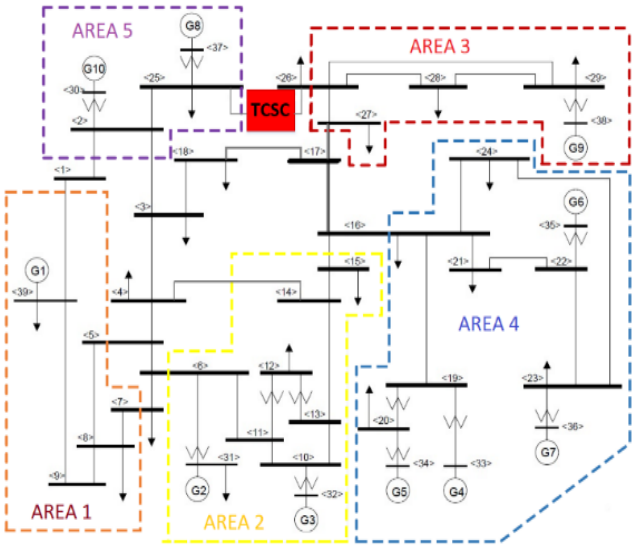


Fig. 19. 39-Bus 10-Machine Power System

TABLE VII
THE INSTALLED PSS ON 39-BUS TEST SYSTEM GENERATORS

Generator	The Installed PSS
G2, G3	$5\frac{8s}{1+8s}\left(\frac{1+0.06s}{1+0.01s}\right)^2$
G9, G8, G5	$7\frac{8s}{1+8s}\left(\frac{1+0.06s}{1+0.01s}\right)^2\left(\frac{1+005s}{1+0.01s}\right)$

TABLE VIII
INTER-AREA MODES OF OSCILLATION OF THE 39-BUS TEST SYSTEM WITH TCSC

Local and inter-area modes value	Mode shape	Damping ratio	Frequency	Mode
$-0.58 \pm 1.76i$	G1 VS. the others	31.29	0.2801	1
$-2.21 \pm 2.52i$	(G3, G2) VS. G9 and (G8,G10)	65.93	0.4010	2
$-1.81 \pm 2.74i$	G9 VS. (G4, G7) and (G8, G10)	55.11	0.4361	3
$-1.64 \pm 4.67i$	(G7, G4) VS. (G2, G3) and (G8,G10)	33.13	0.7432	4

Controllability and observability methods are used to determine the appropriate control location and control signal. One of these methods is the Residue Value which is based on model analysis [30]. This value is calculated for the lines of the case study system, as shown in Table IX. As shown in Table IX, the maximum value of the residues is related to the line (26-25). According to this controllability index, line (26-25) is the best place to install TCSC in this system. The measured signals are the speed of synchronous generators, and the feedback signals are considered the speed difference between the two generators. Also, for a comparative study without TCSC, a wide-area control signal is applied to the input of the AVR system installed on the excitation of some synchronous generators. The selection of the appropriate feedback signal and control location is made independently according to the maximum Geometric Measure of Controllability (GMC) and the maximum Geometric Measure of Controllability (GMO) for that mode to damp the inter-area oscillations. The details of these measures are not discussed here and can be found in [35], while the effectiveness of this method has been confirmed in [32]. Table X shows each mode's control location and selected feedback signal based on the maximum GMC and GMO indices. For example, according to Table 8, the first mode shows the oscillation of the G1 generator compared to the rest of the system generators. It can be effectively controlled by measuring the speed difference between the G1 and G9 generators and applying a control signal to the G9 generator. Therefore, G2, G4, and G9 are the selected control locations to improve the damping of inter-area oscillations. It is also assumed that the bus connected to generators G1, G2, G3, G5, G9, and G10 are equipped with PMUs to obtain feedback signals.

TABLE IX
TCSC RESIDUE COEFFICIENT IN THE 39-BUS TEST SYSTEM

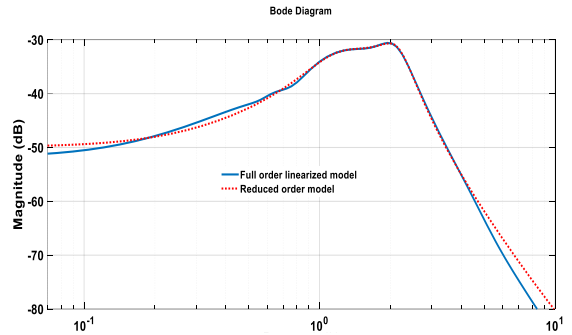
TCSC Placement	
The Normalized Residue	Line
0.34	9 – 39
0.59	17 – 27
0.28	15 – 16
0.91	16 – 21
0.26	14 – 15
0. 58	21 – 22
0.41	16 – 17
0.53	2 – 3
0.13	3 – 4
0.68	2 – 25
0.28	7 – 8
1.00	**25 – 26**
0.52	26 – 28
0.64	28 – 29
0.45	17 – 18

TABLE X
FEEDBACK SIGNALS AND THE SELECTED CONTROL LOCATIONS TO IMPROVE THE DAMPING OF INTER-AREA OSCILLATIONS

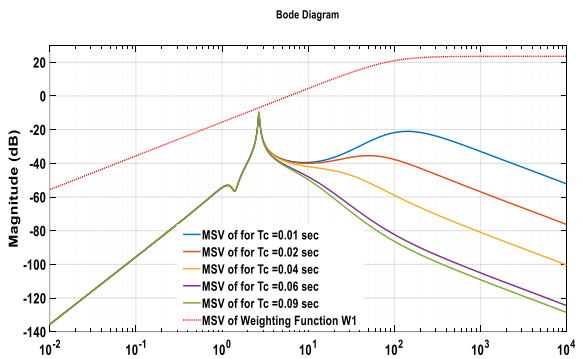
Mode Number	1	2	3	4
Control Location Based on Maximum GMC	G9	G2	G9	G4
Feedback Signal Based on Maximum GMO	$\omega_1 - \omega_9$	$\omega_2 - \omega_9$	$\omega_9 - \omega_{10}$	$\omega_3 - \omega_5$

The linearized model of the case study system is obtained at the nominal operating point using MATLAB software. The order of the obtained linear model is equal to 116. To facilitate the design of the WADC, the order of the system is reduced to

10 using the Schur model order reduction method in the robust control toolbox of MATLAB software. The frequency response of the full-order and the reduced model are shown in Fig. 20 (a). According to this figure, the reduced model has the dynamic behavior of the full-order system with reasonable accuracy in the frequency range of electromechanical modes.



(a)



(b)

Fig. 20. (a) Bode plot of the linearized model and reduced model (b) MSV plot of plant model uncertainty and the corresponding weighting function

As mentioned before, changes in the delay will cause uncertainty in the compensated delay model. The main contribution of the uncertainty is due to the change in the gain of this model. If the GCF is not used to modify the gain value, the gain increases with increasing delay and decreases with decreasing delay. So, the resulted uncertainty can be significantly reduced using an appropriate gain factor. The MSV diagram of the designed plant uncertainty is shown in Fig. 20 (b). The time-varying delay is considered according to Table XI, where θ_τ is a random value between zero and 30ms.

TABLE XI

THE CONSIDERED TIME-VARYING DELAY

Time Interval (s)	Time Delay (ms)
$0 \le t < 7$	$120 \pm \theta_\tau$
$7 \le t < 13$	$300 \pm \theta_\tau$
$13 \le t \le 20$	$480 \pm \theta_\tau$

The maximum and minimum value of the delay for the system is considered 100 ms and 500 ms, respectively. Then, ADCs are designed to compensate for delayed changes adaptively. Therefore, the ADC is installed in the control location, close to the TCSC installation site, to compensate for the delay. The lead-phase time constants of the delay compensator are selected as $T_1 = 01$, $T_2 = 02$, $T_3 = 03$, $T_4 = 04$, $T_5 = 0.5$. Also, the selection of optimal weighting functions $W_1(s)$, $W_2(s)$, and $W_3(s)$ to design the centralized WADC for the 39-bus test system are considered as Eqs. (55)-(57) [32].

$$W_1(s) = \frac{10s}{s+60} \tag{55}$$

$$W_1(s) = \frac{10s}{s+60} \tag{56}$$

$$W_3(s) = \frac{5}{s+10} \tag{57}$$

To design the central controller, the relative weighting factors of a_∞ and a_2 are considered to 0.5 to consider the robustness and efficiency of the controller. In this study, the value of $T_C = 004$ is selected as the ADC lag-phase time constant, and the performance of the designed controller is evaluated. Using small signal analysis for the closed-loop system, the designed controller performance is examined in the face of various delay values and system operating point changes. To define the new operating points, it is assumed that the load of the area containing the G9 and busbars 26, 27, 28, and 29 will change from 60% of the nominal load to 140%. Given that the G9 is involved in all the first three modes, the main purpose of the changes in load and generation is to change the power exchange between the adjacent areas. As shown in Figs. 13 and 14, the proposed WADC improves the damping of inter-area oscillations while its performance does not weaken when confronted with the change in delay value or the operating points.

Time-domain simulations confirm the effectiveness of the presented ADC in the presence of the TCSC. For this purpose, nonlinear simulations are performed for 20 s, and the performance of the proposed method in the face of different values of delay, nonlinear nature of the power system, large disturbances, and changes in operating conditions are evaluated. The proposed method shows excellent damping in different operating conditions and different scenarios of delay changes. Fig. 21 shows the simulation results of a three-phase fault that occurs in 0.1 s between busbars 17 and 18 and clears after 0.1 s. To illustrate the advantage of having a TCSC with an ADC, comparisons are made between WADC with ADC, a DC_5 constant compensator designed for a fixed delay value of 500 ms, and a robust controller provided in [21]. In conventional controllers, the coefficients of the controllers must be changed to keep the system stable by changing the system's operating point, but the ADC and TCSC-based wide-area controller, which is shown in Fig. 22, is robust against load level changes of the system.

According to the time-varying delay scenario presented in Table 10, the moving average of the delay, the weighting factors of the compensators, and control signals with compensated delay (the output of each ADC) applied to the AVR of G2, G4, and G9, which is depicted in Fig. 23. As shown in Fig. 23, the proposed method maintains the desired performance in damping oscillations, and ADC effectively compensates for the time-varying delay. In $0 \leq t < 7$, the average delay is 120 ms and DC_1 can compensate for 100 ms. Therefore, the delay can be partially compensated, and as a result, the performance of DC_1 and ADC is almost the same. As the delay increases during the $t \geq 7$, the uncompensated delay increases significantly, leading to a deterioration in WADC performance.

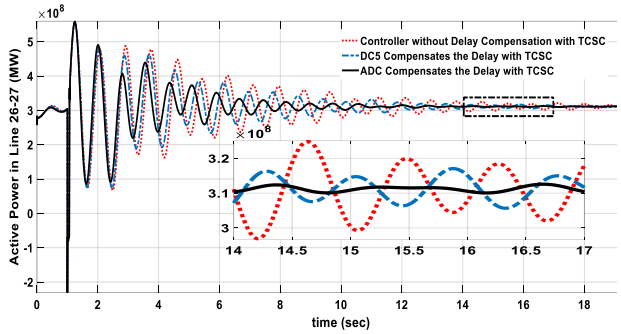
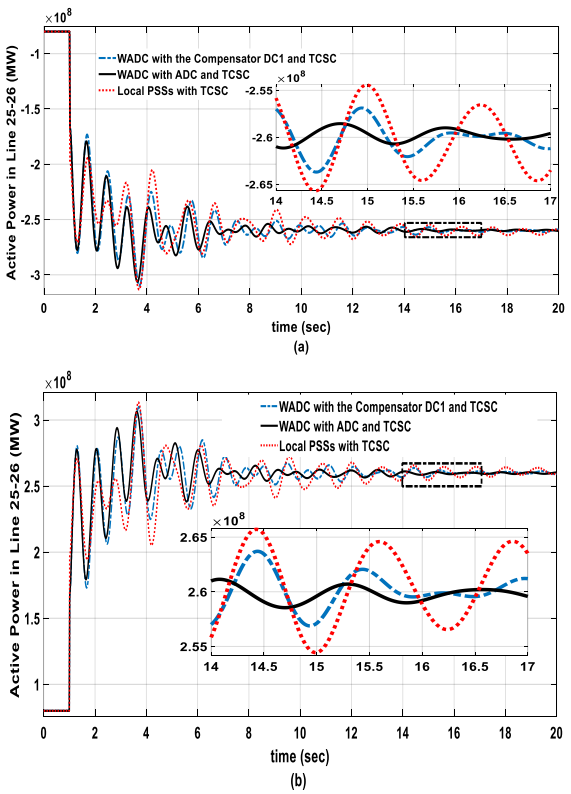


Fig. 21. The occurrence of three-phase fault on line 18-17 and the presence of TCSC between buses 26-25: with ADC - with fixed delay compensator 500ms (DC_5)- No delay compensator



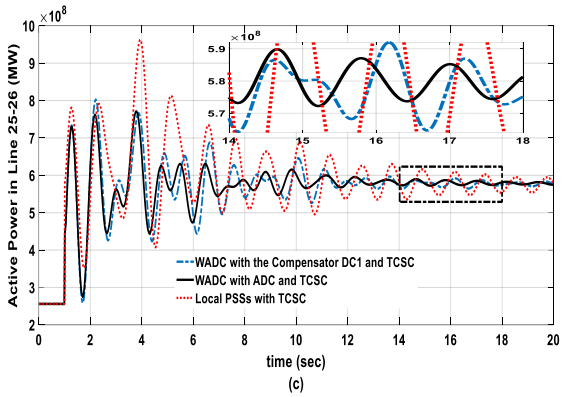
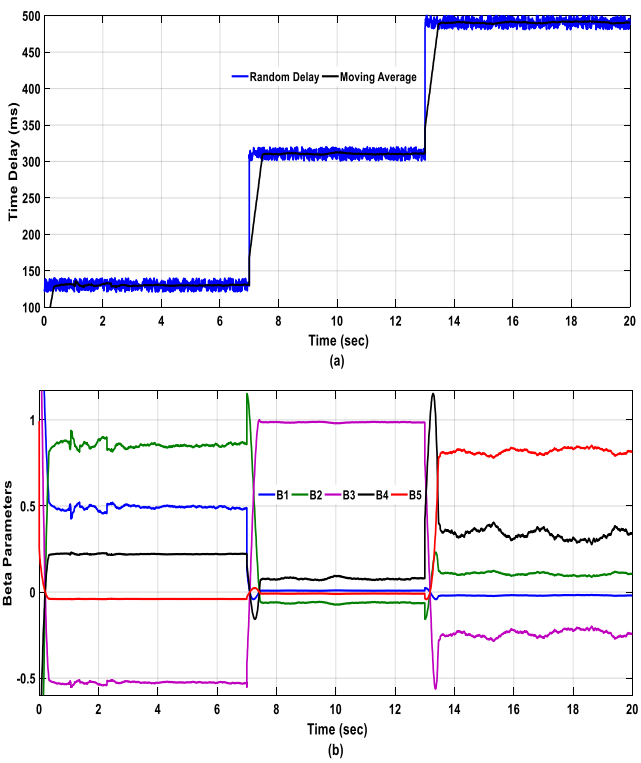
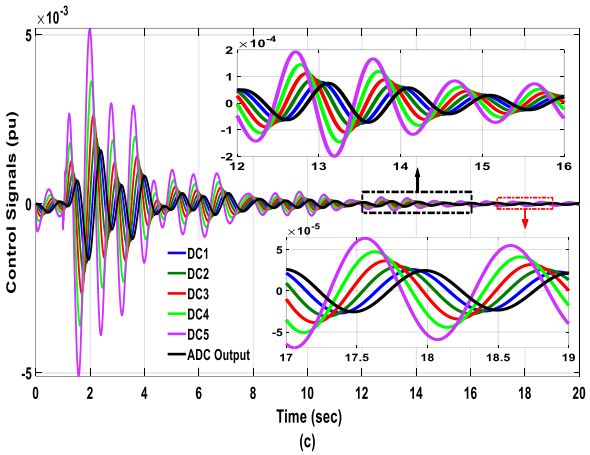


Fig. 22. The occurrence of 3-phase to fault on line 27-17 at different operating points with the presence of TCSC (a) 60% load (b) 100% load (c) 140% load

Also, in Figs. 25 and 26, a comparison of the two cases without TCSC and with TCSC with ADC is considered. When TCSC is used, the wide-area robust control of the system is done in a centralized way (i.e., all feedback signals from the speed difference of the generators are in the same place with WADC and applied to TCSC). Also, when TCSC is not used, the wide-area robust control can be applied semi-centralized, which means at the location of G9, G4, and G2 with PSS signal is applied to the excitation system. Fig. 24 shows the controller analysis against delay changes, while in Fig. 25, the controller is analyzed against load changes.





(c)

Fig. 23. (a) Moving average delay, (b) Changes in compensator weighting factors, and (c) ADC output in the presented scenario in Table IV

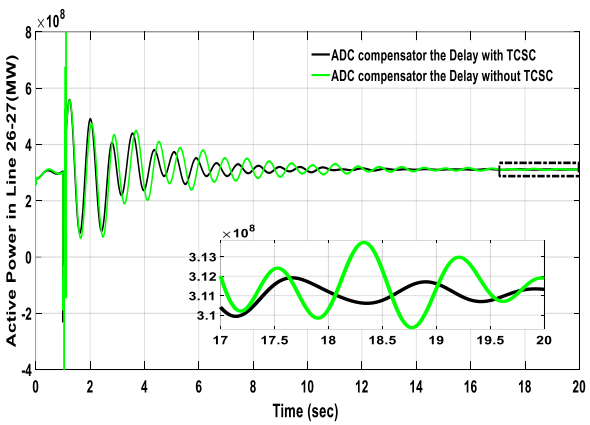
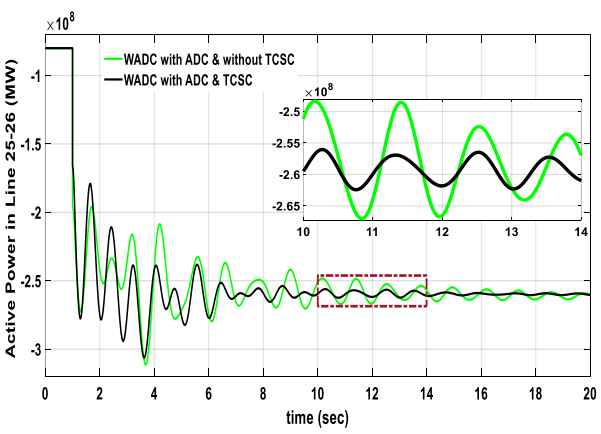
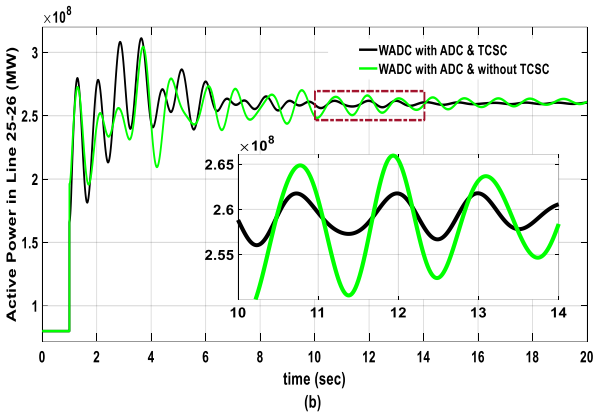


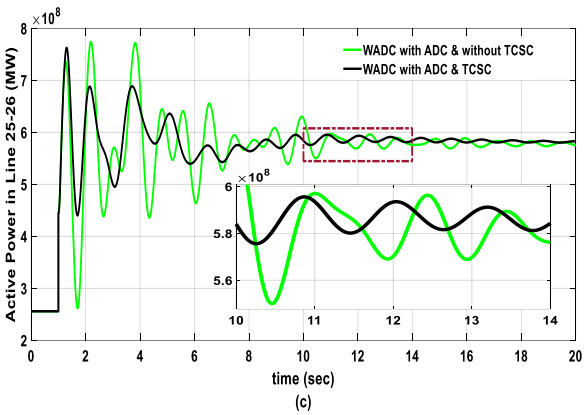
Fig. 24. Comparison of two modes without TCSC and with TCSC considering ADC and delay at different times for 10-machine system and creating three-phase short-circuit fault on line 17-18



(a)



(b)



(c)

Fig. 25. Comparison of two modes without TCSC and with TCSC considering ADC for 39-bus test system and three-phase fault on line 17-27 at different operating points (a) 60% load, (b) 100% load, (c) 140% load

VI. CONCLUSION

This paper presents an ADC to compensate for the time-varying delay in a wide-area robust controller. The proposed adaptive compensator is implemented as the weighted sum of several compensators which each of them has a weighting factor according to the measured delay. Consequently, with the delay variations and compensating for it, these weighting factors are continuously updated. Using this compensator, a model for the compensated delay is presented, which can be easily applied to the system nominal plant to design WADC by the mixed H_2/H_∞ synthesis. Also, the uncertainties in the compensated delay model, caused by delay value variations, have been considered in designing a wide-area controller to ensure its robust stability. Using the simulations carried out on the Two-Area Four-Machine power system, and 39-bus New England test system, the efficiency of the proposed method was investigated by implementing two control schemes based on the use of voltage control loops synchronous generators and the TCSC for damping of the inter-area oscillations. The simulation results confirm the effectiveness of the presented method in compensation for time-varying delay and its robustness against changes in the operating point of the system.

REFERENCES

[1] P. W. Sauer, M.A. Pai, J. H. Chow, *Power System Dynamics and Stability: With Synchro phasor Measurement and Power System Toolbox*, 2th ed., Wiley-IEEE Press, pp. 71-231, 2017.

[2] M. M. Rizi, S. Abazari and N. Mahdian "Dynamic Stability Improvement of Power System with Simultaneous and Coordinated Control of DFIG and UPFC using LMI," *Int. J. Industrial Electronics, Control and Optimization, IECO*, Vol. 4, No.3, pp. 341-353, July. 2021.

[3] P. Agnihotri, A. M. Kulkarni, A. M. Gole, B. A. Archer, and T. Weekes, "A robust wide-area measurement-based damping controller for networks with embedded multiterminal and multi-infeed HVDC links," *IEEE Trans. Power Syst*., vol. 32, no. 5, pp. 3884–3892, 2017.

[4] A. Patel, S. Ghosh, and K. A. Folly, "Inter-area oscillation damping with non-synchronized wide-area power system stabilizer," *IET Gener. Transm. Distrib.*, vol. 12, no. 12, 2018.

[5] G. Tzounas, M. Liu, M. A. Adib Murad, and F. Milano, "Stability Analysis of Wide Area Damping Controllers with Multiple Time Delays," *IFAC-Papers Online*, vol. 51, no. 28, 2018.

[6] M. Mokhtari and F. Aminifar, "Toward wide-area oscillation control through doubly-fed induction generator wind farms," *IEEE Trans. Power Syst.*, vol. 29, no. 6, 2014.

[7] P. Zhang, D. Y. Yang, K. W. Chan, and G. W. Cai, "Adaptive wide-area damping control scheme with stochastic subspace identification and signal time delay compensation," *IET Gener. Transm. Distrib.*, vol. 6, no. 9, 2012.

[8] Y. Li, Y. Zhou, F. Liu, Y. Cao, and C. Rehtanz, "Design and Implementation of Delay-Dependent Wide-Area Damping Control for Stability Enhancement of Power Systems," *IEEE Trans. Smart Grid*, vol. 8, no. 4, 2017.

[9] Y. Li, C. Rehtanz, D. Yang, S. Rüberg, and U. Häger, "Robust high-voltage direct current stabilizing control using wide-area measurement and taking transmission time delay into consideration," *IET Gener. Transm. Distrib.*, vol. 5, no. 3, pp. 289–297, 2011.

[10] D. Dotta, A. S. e Silva, and I. C. Decker, "Wide-area measurements-based two-level control design considering signal transmission delay," *IEEE Trans. Power Syst.*, vol. 24, no. 1, 2009.

[11] W. Yao, L. Jiang, J. Wen, Q. Wu, and S. Cheng, "Wide-area damping controller for power system interarea oscillations: A networked predictive control approach," *IEEE Trans. Control Syst. Technol.*, vol. 23, no. 1, 2015.

[12] H. Ye and Y. Liu, "Design of model predictive controllers for adaptive damping of inter-area oscillations," *Int. J. Electr. Power Energy Syst.*, vol. 45, no. 1, 2013.

[13] L. Cheng, G. Chen, W. Gao, F. Zhang, and G. Li, "Adaptive time delay compensator (ATDC) design for wide-area power system stabilizer," *IEEE Trans. Smart Grid*, vol. 5, no. 6, 2014.

[14] Y. Shen, W. Yao, J. Wen, and H. He, "Adaptive wide-area power oscillation damper design for photovoltaic plant considering delay compensation," *IET Gener. Transm. Distrib.*, vol. 11, no. 18, 2017.

[15] M. Beiraghi and A. M. Ranjbar, "Adaptive Delay Compensator for the Robust Wide-Area Damping Controller Design," *IEEE Trans. Power Syst.*, vol. 31, 2016.

[16] Y. Li, D. Yang, F. Liu, Y. Cao, and C. Rehtanz, *Interconnected Power Systems*, Springer-Verlag Berlin Heidelberg, pp. 93-223, 2016.

[17] R. Fan, S. Wang, R. Huang, J. Lian, and Z. Huang, "Wide-area measurement-based modal decoupling for power system oscillation damping," *Electr. Power Syst. Res.*, vol. 178, 2020.

[18] S. Liu, "Assessing placement of controllers and nonlinear behavior of electrical power system using normal form information," Ph.D. Dissertation, Iowa State University, U.S.A, 2006.

[19] P. Kundur, "*Power system stability and control," Power System Stability and Control*, 3th ed., Wiley-IEEE Press, 2019.

[20] A. Movahedi, A. H. Niasar, and G. B. Gharehpetian, "Designing SSSC, TCSC, and STATCOM controllers using AVURPSO, GSA, and GA for transient stability improvement of a multi-machine power system with PV and wind farms," *Int. J. Electr. Power Energy Syst.*, vol. 106, 2019.

[21] W. Yao, L. Jiang, J. Wen, Q. H. Wu, and S. Cheng, "Wide-area damping controller of Facts devices for inter-area oscillations considering communication time delays," *IEEE Trans. Power Syst.*, vol. 29, no. 1, 2014.

[22] V. V. G. Krishnan, S. C. Srivastava, and S. Chakrabarti, "A robust decentralized wide area damping controller for wind generators and facts controllers considering load model uncertainties," *IEEE Trans. Smart Grid*, vol. 9, no. 1, 2018.

[23] J. Deng, C. Li, and X. P. Zhang, "Coordinated Design of Multiple Robust FACTS Damping Controllers: A BMI-Based Sequential Approach with Multi-Model Systems," *IEEE Trans. Power Syst.*, vol. 30, no. 6, 2015.

[24] I. Abdulrahman, R. Belkacemi, and G. Radman, "Power oscillations damping using wide-area-based solar plant considering adaptive time-delay compensation," *Energy Syst.*, 2019.

[25] S. Ghosh, K. A. Folly, and A. Patel, "Synchronized Versus Non-Synchronized Feedback for Speed-Based Wide-Area PSS: Effect of Time-Delay," *IEEE Trans. Smart Grid*, vol. 9, no. 5, 2018.

[26] N. R. Chaudhuri, S. Ray, R. Majumder, and B. Chaudhuri, "A new approach to continuous latency compensation with adaptive phasor power oscillation damping controller (POD)," *IEEE Trans. Power Syst.*, vol. 25, no. 2, 2010.

[27] X. Zhang, C. Lu, S. Liu, and X. Wang, "A review on wide-area damping control to restrain inter-area low frequency oscillation for large-scale power systems with increasing renewable generation," *Renewable and Sustainable Energy Reviews*, vol. 57. 2016.

[28] M. J. Alinezhad, M. Radmehr, and S. Ranjbar, "Adaptive wide area damping controller for damping inter-area oscillations considering high penetration of wind farms," *Int. Trans. Electr. Energy Syst.*, vol. 30, no. 6, 2020.

[29] M. Mokhtari, F. Aminifar, D. Nazarpour, and S. Golshannavaz, "Wide-area power oscillation damping with a fuzzy controller compensating the continuous communication delays," *IEEE Trans. Power Syst.*, vol. 28, no. 2, 2013.

[30] I. Zenelis and X. Wang, "Wide-area damping control for interarea oscillations in power grids based on PMU measurements," *IEEE Control Syst. Lett.*, vol. 2, 2018.

[31] M. Rydel, R. Stanisławski, and K. J. Latawiec, "Balanced truncation model order reduction in limited frequency and time intervals for discrete-time commensurate fractional-order systems," *Symmetry (Basel).*, vol. 11, no. 2, 2019.

[32] Y. Wang, Q. Wu, W. Gong, and M. P. S. Gryning, "H∞ Robust Current Control for DFIG-Based Wind Turbine Subject to Grid Voltage Distortions," *IEEE Trans. Sustain. Energy*, vol. 8, no. 2, 2017.
[33] Z. Zhang, W. Qiao, and Q. Hui, "Power System Stabilization Using Energy-Dissipating Hybrid Control," *IEEE Trans. Power Syst.*, vol. 34, no. 1, 2019.
[34] Y. Li, C. Rehtanz, S. Rüberg, L. Luo, and Y. Cao, "Wide-area robust coordination approach of HVDC and FACTS controllers for damping multiple interarea oscillations," *IEEE Trans. Power Deliv.*, vol. 27, no. 3, 2012.
[35] M. Li and Y. Chen, "A Wide-Area Dynamic Damping Controller Based on Robust H∞ Control for Wide-Area Power Systems with Random Delay and Packet Dropout," *IEEE Trans. Power Syst*., vol. 33, no. 4, 2018.



Esmaeel Rokrok was born in Khorramabad, Iran, in 1972. He received his B.Sc., M.Sc., and Ph.D. degree in Electrical Engineering from Isfahan University of Technology, in 1985, 1997 and 2010, respectively. He is an associate professor in the Department of Electrical Engineering, Lorestan University. His major research interests lie in the area of power system control and dynamics, dispersed generation, microgrid and robust control.



Saman Dehghaninejad was born in Khorramabad, Iran, in 1995. He received his B.Sc. degree in Electrical Engineering from Semnan University, Semnan, Iran, in 2016, and his M.Sc. in Electrical Engineering from Lorestan University (LU), Khorramabad, Iran, in 2019. He is currently a Ph.D. Student at Lorestan University, Khorramabad, Iran. His research interests include power system control and dynamics, energy management, smart grids.



Amir Hossein Poursaeed was born in Khorramabad, Iran, in 1993. He received B.Sc. and M.Sc. degrees from Lorestan University (LU), Khorramabad, Iran in 2015 and 2018, respectively. He is currently a Ph.D. Student at Lorestan University, Khorramabad, Iran. His research interests include power system protection, stability, electromagnetic transients, and machine learning applications in power systems.